3D Visualization of Macromolecule Synthesis

Timothy J. Duerr[1], Ester Comellas[2,3], Eun Kyung Jeon[1], Johanna E. Farkas[1], Marylou Joetzjer[4], Julien Garnier[4], Sandra J. Shefelbine[3,5], James R. Monaghan[1,*]

[1]Department of Biology, Northeastern University, Boston, MA 02115, USA

[2]Department of Mathematics, Laboratori de Càlcul Numeric (LaCàN), Universitat Politècnica de Catalunya (UPC), 08034 Barcelona, Spain

[3]Mechanical and Industrial Engineering, Northeastern University, Boston, MA 02115, USA

[4]University of Technology of Compiègne, Rue Roger Couttolenc, 60200 Compiègne, France

[5]Department of Bioengineering, Northeastern University, Boston, MA, USA

* Author for correspondence (j.monaghan@northeastern.edu)

Abstract

Measuring nascent macromolecular synthesis *in vivo* is key to understanding how cells and tissues progress through development and respond to external cues. Here, we perform *in vivo* injection of alkyne- or azide-modified analogs of thymidine, uridine, methionine, and glucosamine to label nascent synthesis of DNA, RNA, protein, and glycosylation. Three-dimensional volumetric imaging of nascent macromolecule synthesis was performed in axolotl salamander tissue using whole mount click chemistry-based fluorescent staining followed by light sheet fluorescent microscopy. We also developed an image processing pipeline for segmentation and classification of morphological regions of interest and individual cells, and we apply this pipeline to the regenerating humerus. We demonstrate our approach is sensitive to biological perturbations by measuring changes in DNA synthesis after limb denervation. This method provides a powerful means to quantitatively interrogate macromolecule synthesis in heterogenous tissues at the organ, cellular, and molecular levels of organization.

Introduction

The measurement of nascent DNA, RNA, and protein synthesis in animals provides critical information on the state of cells (dividing, growing, dying) in relation to their surrounding cells. Traditionally, radiolabeled or brominated nucleosides or amino acids are introduced to live animals, where they are incorporated into macromolecules during DNA synthesis[1,2], trancription[3,4], and translation[5]. Performing such approaches have allowed the characterization of cells actively undergoing macromolecular synthesis as well as quantification of synthesis rates, which facilitates the study of cell behavior during tissue remodeling, proliferation, stress, or disease [6-9].

In the past decade, bio-orthogonal macromolecule precursor analogs including 5-ethynyl-2′-deoxyuridine (EdU), 5-ethynyl-uridine (5-EU), and L-azidohomoalanine (AHA) have become commercially available. After injection of macromolecule precursor analogs into animals, precursors can later be detected in nascent DNA, RNA, and protein macromolecules with fluorescently labeled azides or alkynes through highly selective copper catalyzed azide-alkyne cycloaddition (“click”) chemistry[10-12]. These powerful new analogs provide an alternative to the use of dangerous isotopes and the challenges associated with brominated precursors such as the

30 requirement of large secondary antibodies (~150kd) and harsh tissue retrieval methods that limit
31 their use in whole tissue samples.

32 Advantages of the click-chemistry labeling approach include the inert nature of macromolecule
33 precursor analogs that have minimal impact on the animal, the small size of fluorescently labeled
34 alkynes and azides, and the high selectivity of click-chemistry. These advantages have enabled
35 whole mount fluorescent labeling of DNA synthesis[11], RNA transcription[13], protein translation[14],
36 and glycans[15,16] in animals. These pioneering proof of principle experiments have demonstrated
37 that imaging macromolecular synthesis is possible, but the fact that most model organisms are
38 large, optically opaque, and consist of heterogenous tissues has made it a challenge to image
39 biological phenomena in deep tissues. Challenges such as photon penetration, differences in
40 refractive indices among different cellular components, light-induced photodamage, and
41 background fluorescence have limited the use of whole mount imaging of macromolecular
42 synthesis.

43 Advances in light sheet fluorescence microscopes (LSFMs) have recently enabled the imaging of
44 large biological specimens from millimeters to several centimeters in size[17]. LSFMs have been
45 utilized for volumetric imaging of many varieties including visualization of mRNA in whole
46 mount fluorescence *in situ* hybridization experiments[18] and *in vivo* interrogation of deep tissue
47 dynamics in transgenic reporter animals[19] among others[17]. Clearing methods like CLARITY[20],
48 CUBIC[21], and 3DISCO[22] have further enabled volumetric imaging by decreasing refractive index
49 mismatches and tissue clearing to advance large specimen imaging even further. Together, the
50 rise of three-dimensional imaging, new staining techniques, and tissue clearing has demanded
51 new means for cell counting, segmentation, and fluorescence quantification.

52 Here, we present a click-chemistry based method to visualize DNA synthesis, transcription,
53 translation, and protein glycosylation in whole mount samples using LSFM (Figure 1A). We
54 demonstrate the utility of this technique by imaging macromolecular synthesis in the
55 regenerating axolotl salamander limb. Following limb amputation, the axolotl regenerates its
56 limb by generating a mass of proliferating cells at the limb stump called a blastema[23]. The
57 blastema is an ideal environment to test our method because it is an accessible, heterogenous
58 tissue that increases DNA synthesis, transcriptional output, and translation rates compared to

59 uninjured tissue. Furthermore, DNA, RNA, and protein synthesis decrease after denervation of
60 the regenerating limb[24,25].

61 We use the regenerating limb to demonstrate that two click-it ready precursors can be
62 administered and subsequently visualized simultaneously in a single sample. We also show that
63 optical resolution of images can be improved with the clearing agent 2,2'-thiodiethanol (TDE),
64 and that this method works in a number of tissues. We outline an image analysis pipeline for
65 three dimensional (3D) morphology segmentation, cell counting, and fluorescence quantification
66 of stained tissues. We apply this pipeline to the regenerating humerus to demonstrate the
67 multiscale quantitative analysis capabilities of our method. Finally, we show that our method is
68 sensitive enough to detect and quantify changes in DNA synthesis rates in whole mount
69 innervated and denervated regenerating limbs. Taken together, our method provides a unique
70 approach to simultaneously interrogate cell state at the organ, cellular and molecular levels of
71 organization.

72 **Materials and methods**

73 *Animal procedures*

74 Axolotls (*Ambystoma mexicanum*: d/d RRID Catalog #101L) were either bred in captivity at
75 Northeastern University or purchased from the Ambystoma Genetic Stock Center at the
76 University of Kentucky. Experiments were performed in accordance with Northeastern
77 University Institutional Animal Care and Use Committee. Animals were grown to 4-6cm (Mean
78 5.3cm, SD 0.36) and 1-1.5g (Mean 1.3g, SD 0.19g) for use in all studies. For all experiments,
79 animals were anesthetized by treatment of 0.01% benzocaine until visually immobilized. Limbs
80 were amputated either at the distal end of the zeugopod or midway through the stylopod, and
81 bones were trimmed below the amputation plane to allow for uniform growth. At the date of
82 collection, animals were reanaesthetized and injected with either EdU (8.0ng/g animal), 5-EU
83 (270.0µg/g animal), AHA (180.59µg/g animal), or N-azidoacetylglucosamine-tetraacylated
84 (GlcNAz) (4.3µg/g animal) alone or simultaneously with the following combinations:
85 EdU/AHA, EdU/GlcNAz, 5-EU/AHA, 5-EU/GlcNAz. All monomer analogs were purchased
86 from www.clickchemistrytools.com and resuspended in DMSO at the following concentrations:
87 EdU- 300mM, 5-EU- 100mM, AHA- 100mM, GlcNAz- 100mM. Stocks were further diluted in
88 1X phosphate buffered saline (PBS) for injection. Three hours after injection, limbs were

89 collected from the upper stylopod and fixed in 4% paraformaldehyde (PFA) (diluted in 1X PBS)
90 at 4°C overnight. If limbs were denervated, the nerve supply was severed at the brachial plexus
91 24 hours prior to tissue collection.

92 *Whole mount click-it protocol*

93 Following fixation in 4% PFA, samples were washed three times with 1X PBS at room
94 temperature (~23°C) for 5 minutes. Samples were dehydrated in an increasing methanol series at
95 room temperature starting with 25% methanol (diluted in 1X PBS), 50% methanol, 75%
96 methanol, and 100% methanol for 5 minutes at each step. Samples could then be stored in 100%
97 methanol indefinitely at -20°C. For staining, samples were rehydrated in a decreasing methanol
98 series starting with 75% methanol (diluted in 1X PBS), 50% methanol, 25% methanol, and
99 finally placed in 100% 1X PBS for 5 minutes at each step. Samples were then washed 3 times
100 with 1X PBST (1X PBS with 1% Triton) for 5 minutes at room temperature. To aid in clearing,
101 samples were washed in 0.5% trypsin (diluted in 1X PBST) for 30-90 minutes on a rocker at
102 room temperature, or until sample appeared translucent. Samples were washed three times at
103 room temperature for 5 minutes with deionized water, then washed in 100% acetone for 20
104 minutes at -20°C and washed with deionized water again for 10 minutes. Samples were washed
105 in 1X PBST three times at room temperature for 5 minutes prior to applying click-it cocktail for
106 30 minutes at room temperature. The click-it cocktail was made in 1X TRIS buffered saline as
107 follows: 50µL 1M sodium ascorbate (100mM final), 20µL 100mM $CuSO_4$ (4mM final), and 2µL
108 500µM azide- or alkyne-modified Alexa Flour (2µM final), combined in order as listed. After
109 the first round of staining, samples were washed at room temperature 6 times for 30 minutes with
110 rocking. For double-labelling, samples were again placed in the click-it cocktail with a different
111 fluorescent dye to stain for the second analog at room temperature overnight. Both rounds of
112 staining were conducted in the dark to prevent photodegradation of fluorescent molecules. For
113 staining with DAPI, samples were washed 3 times for 5 minutes with 1X PBS, then placed in
114 277mM DAPI for 4 days at room temperature. Samples were washed 3 times for 20 minutes with
115 1X PBS and left in 1X PBS at 4°C for short term storage prior to imaging with LSFM. Whole
116 mount samples were cleared with 67% TDE (diluted in deionized water) overnight at room
117 temperature in the dark.

118 *Tissue section click-it protocol*

119 Following fixation in 4% PFA, samples were washed three times in 1X PBS each for 5 minutes,
120 and cryoprotected in 30% sucrose on a rocker for 1 hour or until the tissue fully sinks. Samples
121 were removed form sucrose and briefly washed in optimal cutting temperature (OCT) compound
122 before mounting in OCT compound and frozen at -80°C. 10µm sections were obtained using a
123 cryostat and baked at 65°C for 15 minutes. Slides were then washed with water for 30 minutes at
124 room temperature to remove residual OCT. Slides were washed once with 1X PBS for 5 minutes
125 at room temperature. The click-it cocktail (same as above) was applied to the slides and
126 incubated at room temperature in the dark for 30 minutes. If staining for a second
127 macromolecule, slides were washed five times for 5 minutes with 1X PBS at room temperature.
128 The samples were then stained for 30 minutes at room temperature in the dark using the above
129 click-it cocktail with a different a fluorophore dye. Following the final click-it reaction, slides
130 were washed once with 1X PBS at room temperature for 5 minutes, then stained with 277mM
131 DAPI for 5 minutes at room temperature. Slides were washed again with 1X PBS for 5 minutes
132 at room temperature and water for 5 minutes at room temperature and mounted with SlowFade™
133 Gold Antifade Mountant (Thermo S36936). Slides were imaged using a Zeiss LSM800 confocal
134 microscope.

135 *Light sheet microscopy*

136 All 3D images were acquired using a Zeiss light sheet Z.1 microscope paired
137 with Zen software. Unless otherwise indicated, samples were cleared and imaged in 67% TDE.
138 Post-processing for visualization purposes was performed with Arivis Vision4D v3.1.4 on
139 a workstation with a 64-bit Windows Embedded Standard operating system, and an Intel(R)
140 Xeon(R) CPU E5-2620 v3 @ 2.40GhZ (2 processors), 128GB RAM, and NVIDIA Quadro
141 K2200 GPU. Sub-volumes were stitched together with the Tile Sorter in Arivis, using the manual
142 projection option. Volume fusion was performed through automatic landmark registration of
143 manually selected points for alignment. Finally, constant background intensity was corrected
144 using the automatic functionality.

145 *Data analysis*

146 All data were processed on desktop computers with the aid of Fiji[26] and Matlab[27]. The custom
147 Fiji scripts and Matlab codes used are available in the supplementary material. We performed all
148 analyses on unprocessed .czi files acquired directly from the light sheet microscope.

149 Organ level: The goal of the organ level analysis was to determine gross morphology of the
150 organ, such as area, principal axes, and maximum diameters in said axes for each cross section.
151 Critical to this step is alignment of the images to a standard defined axis and reslicing in the
152 transverse direction (perpendicular to the long axis of the humerus). The image stack of a
153 regenerating axolotl elbow was imported into Fiji and aligned along the proximodistal axis of the
154 humerus (Figure 3A). Morphological segmentation of the humerus was performed semi-
155 automatically with the Segmentation Editor plugin (Figure 3B). The segmented surface was then
156 exported from Fiji as a mesh via an .stl file using 3D Viewer[28]. Volumetric analysis was
157 performed in Fiji by reslicing the aligned mask (Figure 3B) to obtain a stack of cross-sections
158 perpendicular to the proximodistal axis, and then quantified the shape and volume with the Slice
159 Geometry option in the BoneJ[29] Fiji plugin. Slice Geometry calculates cross-sectional geometric
160 properties of shapes, including area, second moment of area around the major and minor axes,
161 and maximum chord length from these major and minor axes.

162 Cellular level: The goal of the cellular level analysis was to determine the number of
163 proliferating cells (EdU^+) as a function of proximodistal position along the humerus, as well as
164 average size, shape, and orientation. The aligned image stack (Figure 3A) was cropped using the
165 morphological segmentation (Figure 3B) as a mask with the aid of the Image Calculator in Fiji.
166 Based on the EdU staining (Figure 3C), we segmented the nuclei of the proliferating cells with
167 Trainable Weka Segmentation 3D[30]. We used a combination of filters available in Fiji before and
168 after training the algorithm to improve segmentation results. Filters applied include the 3D Edge
169 and Symmetry, Background Subtraction, 3D Fill Holes, Gaussian Blur 3D, and 3D Watershed
170 Split. A detailed description of the sequence and parameters used is available in the
171 supplementary materials. The 3D Objects Counter then provided a list of identified cells as well
172 as their volume and position, among other information. In addition, the surfaces of the
173 segmented cell nuclei were exported and processed in MeshLab, similarly to the process
174 followed with the organ segmentation, to be visualized in Matlab (Figure 3E). The centroid
175 coordinates and corresponding object volumes identified in Fiji were imported into Matlab for
176 further processing and plotting. We computed the number of cell centroids within 50μm thick
177 slices perpendicular to the proximodistal axis to obtain a density-like measure of proliferating
178 cells. Slice thickness was selected as slightly larger than the average cell diameter to ensure cells
179 were not sampled across more than two slices.

180 Molecular level: The goal of the molecular level analysis was to determine molecular activity,
181 characterized by fluorescent signal, which in our study represented DNA replication (EdU). The
182 aligned and cropped image stack used as a starting point of the cellular-level analysis (Figure
183 3C) was also analyzed at the molecular level. We resliced the image stack along the
184 proximodistal axis in the organ under study (Figure 3F). The histogram and pixel intensity
185 statistics were listed for each slice via the getRawstatistics function. These allow for further
186 quantification of the fluorescent signal in Matlab, e.g. we calculated the mean intensity of each
187 plane along the proximodistal axis and the histogram of the whole organ. For the example
188 showing nerve-dependent regeneration in axolotl blastemas (Figure 6A), we compared overall
189 pixel intensity of the left (denervated) and right (control, innervated) forelimbs of the same
190 animal. To ensure full repeatability of our data analysis, we selected the same cubic volume in all
191 blastemas processed: a cube with 175µm sides, centered along the proximal-distal axis and at a
192 distance of 250µm from the distal tip (Figure 6A). The cube size was adjusted to maximize the
193 cube volume for all blastemas processed, while ensuring that the entire cube was contained
194 within the blastema. Histograms of each cubic volume and the ratio between the innervated and
195 denervated limb of the same animal were computed and plotted with Matlab (Figure 6B) to
196 quantify the changes in proliferation in innervated versus denervated limbs at different stages of
197 regeneration. All scripts for blastema cube quantification are provided in the supplementary
198 materials.

199 **Results and discussion**

200 *Whole mount, click-it based visualization of macromolecule synthesis*

201 To visualize macromolecule synthesis, we injected click-it compatible monomer analogs (Table
202 1) intraperitonially three hours prior to sample collection. During this time, analogs
203 metabolically incorporated into nascently synthesized macromolecules, resulting in *in vivo*
204 labeling of macromolecule synthesis. These labeled macromolecules contain either azide- or
205 alkyne-modified monomers that can be detected with click-it compatible fluorescent molecules,
206 enabling imaging of nascent macromolecules in whole mount tissues with LSFM (Figure 1). To
207 demonstrate the multiplexing capabilities of the approach, modified monomer analogs with
208 disparate functional groups (EdU/AHA, 5-EU/AHA, EdU/GlcNAz, 5-EU/GlcNAz) were co-
209 injected and visualized with LSFM (Figure 2A-D, Supplementary videos 1-2). Whole mount

210 samples were comparable to 2D longitudinal tissue sections of the same stains (Figure 2I-L),
211 showing that our method generates similar results in both whole mount and tissue sections
212 (Supplementary Figure 1). We demonstrate the specificity of N-Acetylglucosamine (GlcNAc)
213 incorporation by showing that a GlcNAz-specific antibody pretreated on tissue sections collected
214 from GlcNAz injected animals prevented the subsequent click-it reaction (Supplementary Figure
215 2).

216 An advantage of our method is that staining whole mount tissues eliminates the need for
217 sectioning, reducing the potential inconsistences that arise as a result of the sectioning process
218 (uneven tissue, different cutting planes, etc.). Additionally, traditional methods of obtaining 3D
219 images of thick tissues with confocal microscopy are impractically slow when imaging hundreds
220 of images in a single stack. LSFM allows for more rapid imaging of whole samples, requiring
221 only minutes to image each sample. However, several considerations exist when imaging whole
222 tissue in 3D with LSFM. Stain penetrates slower in whole 3D tissues compared to 10-20µm thick
223 tissue sections, requiring longer staining times. An advantage of our method is that the click
224 reaction requires molecularly diminutive reagents that readily pass through cell and nuclear
225 membranes, ensuring stain penetration in the center of dense tissues. Different refractive indices
226 between disparate cellular components and the imaging media cause light to scatter, which can
227 reduce the resolution and brightness of 3D images[31]. To improve image resolution and light
228 penetration, overnight refractive index matching with 67% 2,2'-thiodiethanol (TDE) can
229 sufficiently clear axolotl limbs for imaging with LSFM. This clearing method rapidly and
230 effectively improves the signal to noise ratio of stained samples compared to imaging in PBS
231 (Supplementary Figure 3). With careful attention to these challenges, our method provides a
232 means to obtain high quality 3D images from tissues 1mm in depth in less than 10 minutes per
233 sample (Figure 2A-H) with clear, consistent staining.

234 *3D, multiscale quantitative analysis of the regenerating humerus*

235 To demonstrate that our whole mount click-it method can obtain quantifiable data on the organ,
236 cellular, and molecular levels of organization, we applied our technique to the regenerating
237 humerus. After regenerating for 35 days, axolotls with mid-humeral amputations were injected
238 with EdU/AHA to identify cells within the humerus undergoing DNA synthesis (EdU) and
239 protein translation (AHA). We observed EdU staining in chondrocytes distal to the amputation

240 plane and AHA staining in the humerus perichondrium (Figure 3A). We outline a multiscale,
241 quantitative pipeline that leverages the staining patterns of these macromolecules for analysis of
242 3D humerus morphology and 3D macromolecule synthesis. This workflow combines available
243 plugins in Fiji[26] and scripts developed in Fiji and Matlab[27] for the data analysis process (see
244 supplementary information for a detailed description).

245 For 3D organ level analysis of macromolecule synthesis, AHA staining provided an adequate
246 outline of the humerus, allowing us to segment its 3D morphology (Figure 3A-B). We quantified
247 organ shape by assessing cross-sectional area (Figure 4A') and circularity (Figure 4A") of the
248 segmented humerus along the proximodistal axis with BoneJ[29] (Figure 4A). These measurements
249 of 3D organ size can be obtained with other methods such as microCT and focused ion beam
250 scanning electron microscopy (FIB-SEM). However, microCT is unable to image every tissue
251 due to stain limitations and uses hazardous radiation, while FIB-SEM can capture 3D surface
252 topography but not the entire organ morphology. Our method has the capability to fully image
253 the 3D structure of entire organs (size permitting) without the need for radiation while
254 simultaneously capturing information from both the cellular and molecular levels of
255 organization.

256 On the cellular level, we segmented the 3D morphology of proliferating chondrocytes based on
257 EdU staining using the Trainable Weka Segmentation 3D plugin[30] (Figure 4B"). With this
258 segmentation, we identify highly condensed regions of cells undergoing rapid rates of DNA
259 synthesis (Figure 4B). From these data, we observe cells synthesizing DNA most abundantly
260 distal to the plane of amputation, as expected for dividing chondrocytes. Traditionally, cell
261 quantification as such is conducted on 2D tissue sections. In heterogenous tissues, however, cells
262 are distributed non-uniformly; 2D sampling may not accurately capture the cellular distribution
263 and cannot be used to determine cell volume or shape. Our whole mount staining method allows
264 quantification of cells within an entire 3D tissue, resulting in a more accurate assessment of cell
265 density within heterogenous tissues.

266 To demonstrate quantitative molecular analysis of 3D macromolecule synthesis, we assessed
267 staining intensity of EdU in slices along the proximodistal axis of the regenerating humerus (Fig
268 4C). EdU intensity represents the rate at which a cell undergoes DNA synthesis, which is one of
269 the first steps of cell division and proliferation. Proliferating cells rapidly synthesize DNA,

270 enabling cells to integrate EdU into nascent DNA strands, providing ample opportunities for
271 covalent linkage of fluorescent molecules to the DNA strand. Thus, higher pixel values within
272 EdU^+ cells are representative of faster DNA synthesis rates. These data show that EdU intensity
273 is strongest in the regions distal to the amputation plane of the humerus (Figure 4C'), providing a
274 quantitative measure to assess macromolecule synthesis on the molecular level. Within a tissue,
275 cells synthesize macromolecules heterogeneously, reflected by different fluorescence values
276 between cells. Thus, quantifying macromolecule synthesis based on presence/absence of signal
277 instead of fluorescence does not account for variability in macromolecule synthesis rates among
278 cells. To compound this issue, quantifying fluorescence in tissue sections only represents the rate
279 of macromolecule synthesis from a fraction of cells in larger, heterogenous tissues. Our method
280 provides a means to capture this molecular heterogeneity in 3D samples, allowing us to observe
281 whole 3D regions in the regenerating humerus that synthesize DNA more rapidly than others,
282 which further demonstrates the utility of our whole mount click staining method.

283 Taken together, these results demonstrate that our method can provide quantifiable data on the
284 organ, cellular, and molecular levels of organization. This highlights the novelty of our method,
285 as we have not found previous examples of multiscale analysis as outlined here. We foresee this
286 multiscale, quantitative analysis having broad applications in the examination of dynamic cell
287 processes in 3D, such as in cancer metabolism and mammalian neurogenesis or other fields
288 where macromolecule synthesis is traditionally studied in tissue sections.

289 *3D, molecular analysis of biological perturbations*

290 To demonstrate that our method is sensitive enough to detect subtle changes in macromolecule
291 synthesis in vivo, we quantified the difference in EdU intensity between limbs regenerating with
292 and without a nerve supply. Cell proliferation in regenerating limbs is sustained by factors
293 secreted from nerves that innervate the limb[32,33]. Therefore, we amputated both forelimbs at the
294 mid-humerus, and the left limb was denervated at the brachial plexus one day prior to collection.
295 At 6, 9, 12, 15, 18, and 25 days post amputation (dpa) animals were pulsed with EdU for 3 hours
296 before collection to label proliferating blastema cells (Figure 5A). LSFM was used to image
297 samples (Figure 5B), ensuring pixel resolution was consistent between samples. We quantified
298 DNA synthesis in denervated limbs compared to innervated limbs by creating a 175x175x175µm
299 cube 250µm from the distal most tip of the blastema (Figure 6A). From these results, we

300 observed a marked decrease in blastema EdU incorporation due to denervation at 9, 12, and
301 15dpa (Figure 6B), demonstrating that our whole mount staining approach is capable of detecting
302 changes in macromolecule synthesis after biological perturbations. One potential limitation of
303 our method in the blastema is the inability to preform single cell segmentation. We predict that
304 imaging with higher magnification may overcome this limitation but will significantly increase
305 imaging time and file size.

306 **Conclusions**

307 The work presented here provides a fast, simple pipeline for visualizing macromolecule turnover
308 in the 3D space of whole tissues. While tissue sections were previously the standard for studying
309 these cellular processes, a new standard in the field must be expected where dynamic processes
310 like macromolecule synthesis are visualized in 3D to obtain a more complete understanding of
311 how these processes occur in a larger tissue context. Few modalities of imaging exist to provide
312 this level of analysis. Here, we outline a method to study macromolecule synthesis at the organ,
313 cellular, and molecular levels of organization, which is important in understanding cell state and
314 how cell state affects neighboring cells and tissues. To this end, we show that DNA synthesis,
315 transcription, translation, and protein glycosylation increase in the entire 3D space of the
316 regenerating blastema after limb amputation and that these processes can be visualized
317 concurrently. We outline a multiscale pipeline for analysis and quantification of heterogeneous
318 tissues at the organ, cellular, and molecular levels of organization. Additionally, we demonstrate
319 that our method is sensitive to detect biological perturbations by showing a decrease in DNA
320 synthesis in the blastema following limb denervation. We foresee our method being used to
321 similarly readdress other classical questions with modern techniques for a more exhaustive
322 understanding of biological processes; traditional questions within the fields of cancer biology
323 and neurobiology may especially benefit from a technology as such. Additionally, as more click-
324 it ready macromolecules monomer analogs are generated, our method will provide a means to
325 study more biological processes in whole tissues.

326 **Acknowledgements**

327 The authors would like to acknowledge Tyler Jensen for his early assistance in developing the
328 whole mount staining protocol, and both Alex Lovely and Gouxin Rong for their microscopy and
329 image analysis assistance. Images obtained from the Harvard University Center for Biological

Imaging and the Northeastern University Chemical Imaging of Living Systems core. We acknowledge animal support from the Ambystoma Genetic Stock Center funded by NIH grant P40-OD019794.

Author Contributions

SJS and JRM conceived and supervised the study. TJD, EKJ, and JEF preformed experiments and imaging. EC, MJ, and JG designed and implemented codes for multiscale data analysis. TJD and EC performed the analysis. TJD, EC, SJS, and JRM wrote the paper. All authors approved the final version of the manuscript.

Funding

This project has received funding from the National Science Foundation under grant #1727518 to SJS, #1656429 and #1558017 to JRM. E.C acknowledges funding from the European Union's Horizon 2020 research and innovation program under the Marie Skłodowska-Curie grant agreement No. 841047. EKJ acknowledges support from a Northeastern University Matz Scholarship and Undergraduate Research Fellowship.

Competing interests

The authors declare no competing or finical interests.

346 **References**

347 1 Sidman, R. L., Miale, I. L. & Feder, N. Cell proliferation and migration in the primitive
348 ependymal zone: an autoradiographic study of histogenesis in the nervous system. *Exp*
349 *Neurol* **1**, 322-333, doi:10.1016/0014-4886(59)90024-x (1959).
350 2 Gratzner, H. G. Monoclonal antibody to 5-bromo- and 5-iododeoxyuridine: A new
351 reagent for detection of DNA replication. *Science* **218**, 474-475,
352 doi:10.1126/science.7123245 (1982).
353 3 Uddin, M., Altmann, G. G. & Leblond, C. P. Radioautographic visualization of
354 differences in the pattern of [3H]uridine and [3H]orotic acid incorporation into the RNA
355 of migrating columnar cells in the rat small intestine. *J Cell Biol* **98**, 1619-1629,
356 doi:10.1083/jcb.98.5.1619 (1984).
357 4 Wansink, D. G. *et al.* Fluorescent labeling of nascent RNA reveals transcription by RNA
358 polymerase II in domains scattered throughout the nucleus. *J Cell Biol* **122**, 283-293,
359 doi:10.1083/jcb.122.2.283 (1993).
360 5 Garlick, P. J., McNurlan, M. A. & Preedy, V. R. A rapid and convenient technique for
361 measuring the rate of protein synthesis in tissues by injection of [3H]phenylalanine.
362 *Biochem J* **192**, 719-723, doi:10.1042/bj1920719 (1980).
363 6 Yoshizawa, F., Nagasawa, T., Nishizawa, N. & Funabiki, R. Protein synthesis and
364 degradation change rapidly in response to food intake in muscle of food-deprived mice. *J*
365 *Nutr* **127**, 1156-1159, doi:10.1093/jn/127.6.1156 (1997).
366 7 Rombouts, Y. *et al.* Acute phase inflammation is characterized by rapid changes in
367 plasma/peritoneal fluid N-glycosylation in mice. *Glycoconj J* **33**, 457-470,
368 doi:10.1007/s10719-015-9648-9 (2016).
369 8 Brien, T. & Lis, J. T. Rapid changes in Drosophila transcription after an instantaneous
370 heat shock. *Mol Cell Biol* **13**, 3456, doi:10.1128/MCB.13.6.3456 (1993).
371 9 Rose, R. J., Cran, D. G. & Possingham, J. V. Changes in DNA synthesis during cell
372 growth and chloroplast replication in greening spinach leaf disks. *J Cell Sci* **17**, 27-41
373 (1975).
374 10 Kolb, H. C., Finn, M. G. & Sharpless, K. B. Click Chemistry: Diverse Chemical Function
375 from a Few Good Reactions. *Angew Chem Int Ed Engl* **40**, 2004-2021, doi:10.1002/1521-
376 3773(20010601)40:11<2004::aid-anie2004>3.3.co;2-x (2001).
377 11 Salic, A. & Mitchison, T. J. A chemical method for fast and sensitive detection of DNA
378 synthesis in vivo. *Proc Natl Acad Sci U S A* **105**, 2415-2420,
379 doi:10.1073/pnas.0712168105 (2008).
380 12 Best, M. D. Click chemistry and bioorthogonal reactions: unprecedented selectivity in the
381 labeling of biological molecules. *Biochemistry* **48**, 6571-6584, doi:10.1021/bi9007726
382 (2009).
383 13 Jao, C. Y. & Salic, A. Exploring RNA transcription and turnover in vivo by using click
384 chemistry. *Proc Natl Acad Sci U S A* **105**, 15779-15784, doi:10.1073/pnas.0808480105
385 (2008).
386 14 Hinz, F. I., Dieterich, D. C., Tirrell, D. A. & Schuman, E. M. Non-canonical amino acid
387 labeling in vivo to visualize and affinity purify newly synthesized proteins in larval
388 zebrafish. *ACS Chem Neurosci* **3**, 40-49, doi:10.1021/cn2000876 (2012).
389 15 Sawa, M. *et al.* Glycoproteomic probes for fluorescent imaging of fucosylated glycans in
390 vivo. *Proc Natl Acad Sci U S A* **103**, 12371-12376, doi:10.1073/pnas.0605418103 (2006).

16 Laughlin, S. T. & Bertozzi, C. R. Imaging the glycome. *Proc Natl Acad Sci U S A* **106**, 12-17, doi:10.1073/pnas.0811481106 (2009).
17 Power, R. M. & Huisken, J. A guide to light-sheet fluorescence microscopy for multiscale imaging. *Nat Methods* **14**, 360-373, doi:10.1038/nmeth.4224 (2017).
18 Mano, T. *et al.* Whole-Brain Analysis of Cells and Circuits by Tissue Clearing and Light-Sheet Microscopy. *J Neurosci* **38**, 9330-9337, doi:10.1523/jneurosci.1677-18.2018 (2018).
19 Tomer, R., Khairy, K., Amat, F. & Keller, P. J. Quantitative high-speed imaging of entire developing embryos with simultaneous multiview light-sheet microscopy. *Nature Methods* **9**, 755-763, doi:10.1038/nmeth.2062 (2012).
20 Chung, K. *et al.* Structural and molecular interrogation of intact biological systems. *Nature* **497**, 332-337, doi:10.1038/nature12107 (2013).
21 Susaki, E. A. *et al.* Whole-brain imaging with single-cell resolution using chemical cocktails and computational analysis. *Cell* **157**, 726-739, doi:10.1016/j.cell.2014.03.042 (2014).
22 Erturk, A. *et al.* Three-dimensional imaging of solvent-cleared organs using 3DISCO. *Nat Protoc* **7**, 1983-1995, doi:10.1038/nprot.2012.119 (2012).
23 Stocum, D. L. Mechanisms of urodele limb regeneration. *Regeneration* **4**, 159-200, doi:10.1002/reg2.92 (2017).
24 Singer, M. & Caston, J. D. Neurotrophic dependence of macromolecular synthesis in the early limb regenerate of the newt, <em>Triturus</em&gt. *Journal of Embryology and Experimental Morphology* **28**, 1 (1972).
25 Dresden, M. H. Denervation effects on newt limb regeneration: DNA, RNA, and protein synthesis. *Dev Biol* **19**, 311-320, doi:10.1016/0012-1606(69)90044-x (1969).
26 Schindelin, J. *et al.* Fiji: an open-source platform for biological-image analysis. *Nature Methods* **9**, 676-682, doi:10.1038/nmeth.2019 (2012).
27 MATLAB version 9.7.0.813654 (R2019b). Natick, Massachusetts: The MathWorks Inc.; 2019
28 Pietzsch, T., Saalfeld, S., Preibisch, S. & Tomancak, P. BigDataViewer: visualization and processing for large image data sets. *Nature Methods* **12**, 481-483, doi:10.1038/nmeth.3392 (2015).
29 Doube, M. *et al.* BoneJ: Free and extensible bone image analysis in ImageJ. *Bone* **47**, 1076-1079, doi:10.1016/j.bone.2010.08.023 (2010).
30 Arganda-Carreras, I. *et al.* Trainable Weka Segmentation: a machine learning tool for microscopy pixel classification. *Bioinformatics* **33**, 2424-2426, doi:10.1093/bioinformatics/btx180 (2017).
31 Fadero, T. C. & Maddox, P. S. Live imaging looks deeper. *Elife* **6**, e30515, doi:10.7554/eLife.30515 (2017).
32 Singer, M. The influence of the nerve in regeneration of the amphibian extremity. *Q Rev Biol* **27**, 169-200, doi:10.1086/398873 (1952).
33 Farkas, J. E. & Monaghan, J. R. A brief history of the study of nerve dependent regeneration. *Neurogenesis (Austin)* **4**, e1302216, doi:10.1080/23262133.2017.1302216 (2017).

434 **Table 1. Monomer analogs used to demonstrate whole mount visualization method**

Name	Macromolecule analog	Biological process	Click-it modification	Reference
5-ethynyl-2′-deoxyuridine (EdU)	Thymidine	DNA synthesis	Alkyne	Salic & Mitchison 2008
5-Ethynyl Uridine (5-EU)	Uracil	Transcription	Alkyne	Jao & Salic 2008
L-Azidohomoalanine (AHA)	Methionine	Translation	Azide	Wang et al. 2017
Azide-modified glucosamine (GlcNAz)	Glucoseamine	Protein glycosylation	Azide	Laughlin et al. 2006

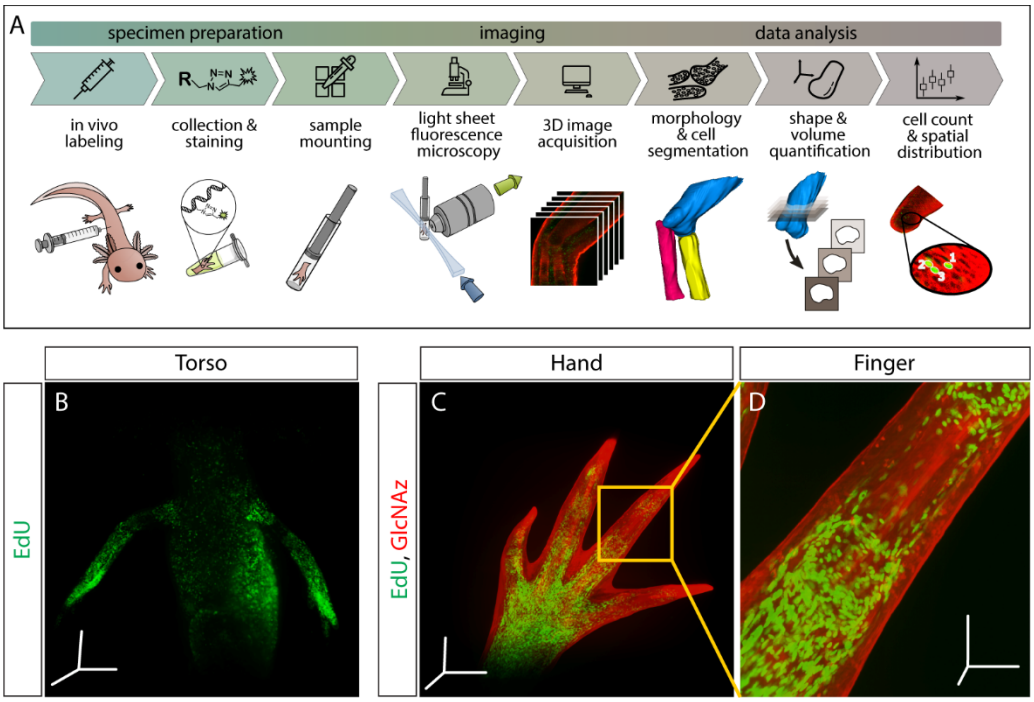

435 **Figure 1. Outline of staining/analysis pipeline and exemplary images.**

436 (A) Overview of entire sample preparation, imaging, and data analysis pipeline. (B-D) Once
437 macromolecules are labeled *in vivo*, synthesis can be visualized throughout the injected animal.
438 Here, we show DNA synthesis (EdU) in the torso (B) and both DNA synthesis and protein
439 glycosylation (GlcNAz) in the hand (C) and finger (D). Images from panels B and C were
440 uncleared and imaged at 5X magnification. Image from panel D was also uncleared and imaged
441 at 10X magnification. Scale bars for panels B&C= 600µm for each axis. Scale bars for panel D=
442 200µm for each axis.

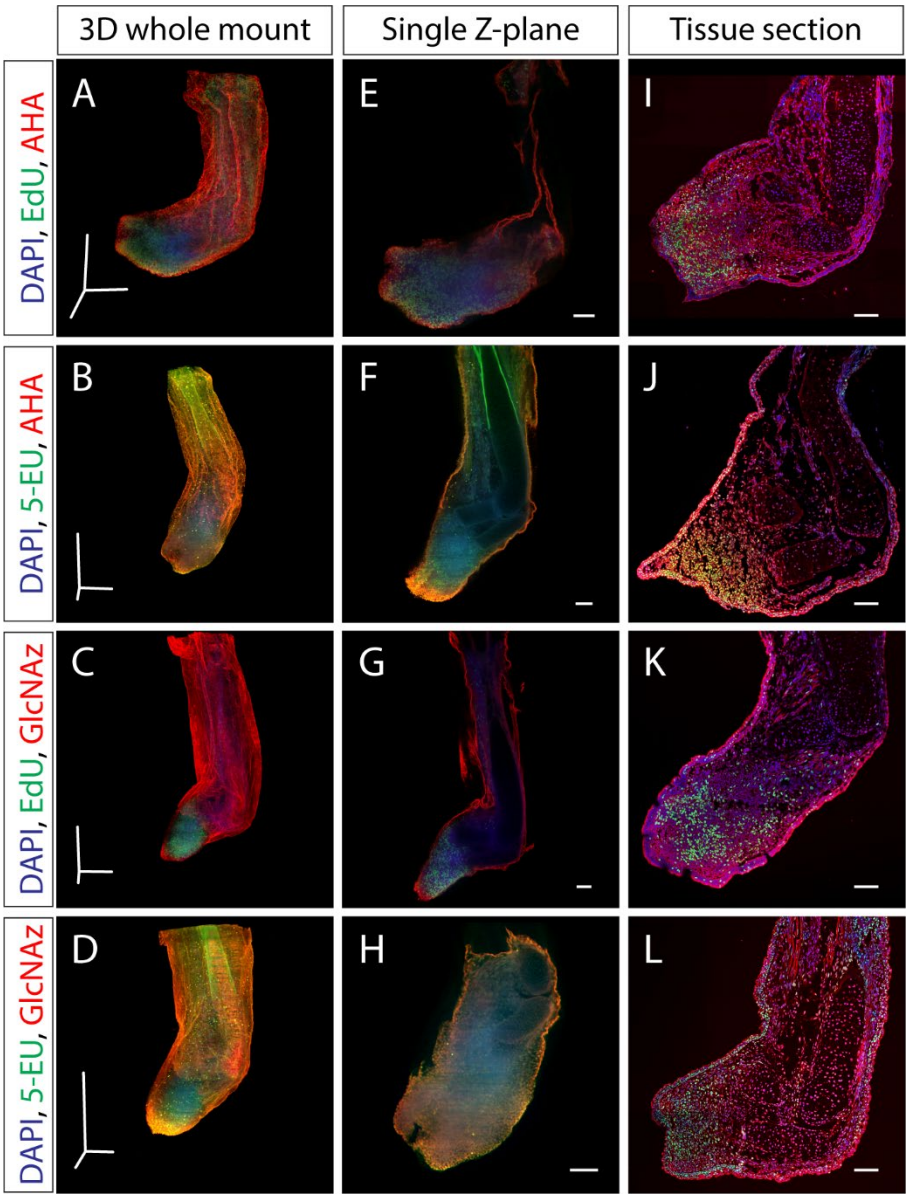

Figure 2. Dual staining of macromolecule synthesis in whole mount.

(A-D) Stitched and fused 3D reconstruction of 13 dpa blastemas stained for multiple macromolecules obtained by LSFM. (B-H) Single Z-plane from A-D that represents the entirety of the blastema. (I-L) Tissue section from identically treated limbs as A-H showing similar macromolecule staining patterns, indicating that the whole mount staining method does not alter macromolecule synthesis staining patterns. Scale bars for panels A-D= 600µm for each axis. Scale bars for panels E-L= 200µm.

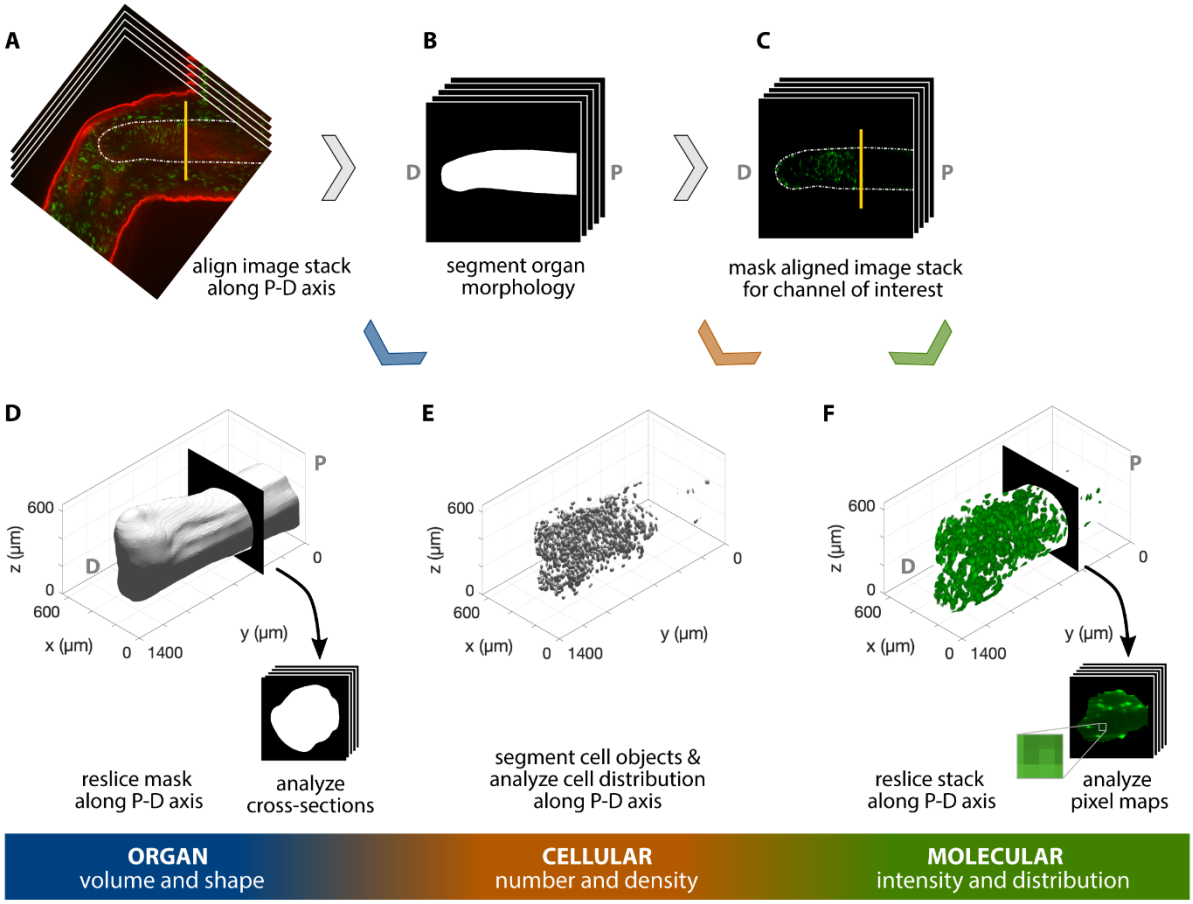

Figure 3. Workflow for 3D, multiscale analysis of the regenerating axolotl humerus.

Multiscale analysis of a 35 dpa regenerating axolotl humerus, stained for AHA (red) and EdU (green). The humerus in the image stack was (A) aligned along the proximodistal (P-D) axis and (B) its morphology was segmented. The resulting mask was used to analyze the organ volume and shape by (D) reslicing it along the P-D axis and studying the cross-sections obtained. (C) The segmented morphology in B was used to mask the green channel for cellular- and molecular-level analyses. (E) Cells in the humerus were segmented and their spatial distribution was analyzed to obtain cellular number and density. (F) The masked image stack in C was resliced along the P-D axis and the pixel maps of the cross-sections were used to characterize the molecular intensity and distribution within the humerus. The vertical yellow line in A and C indicates the plane of amputation.

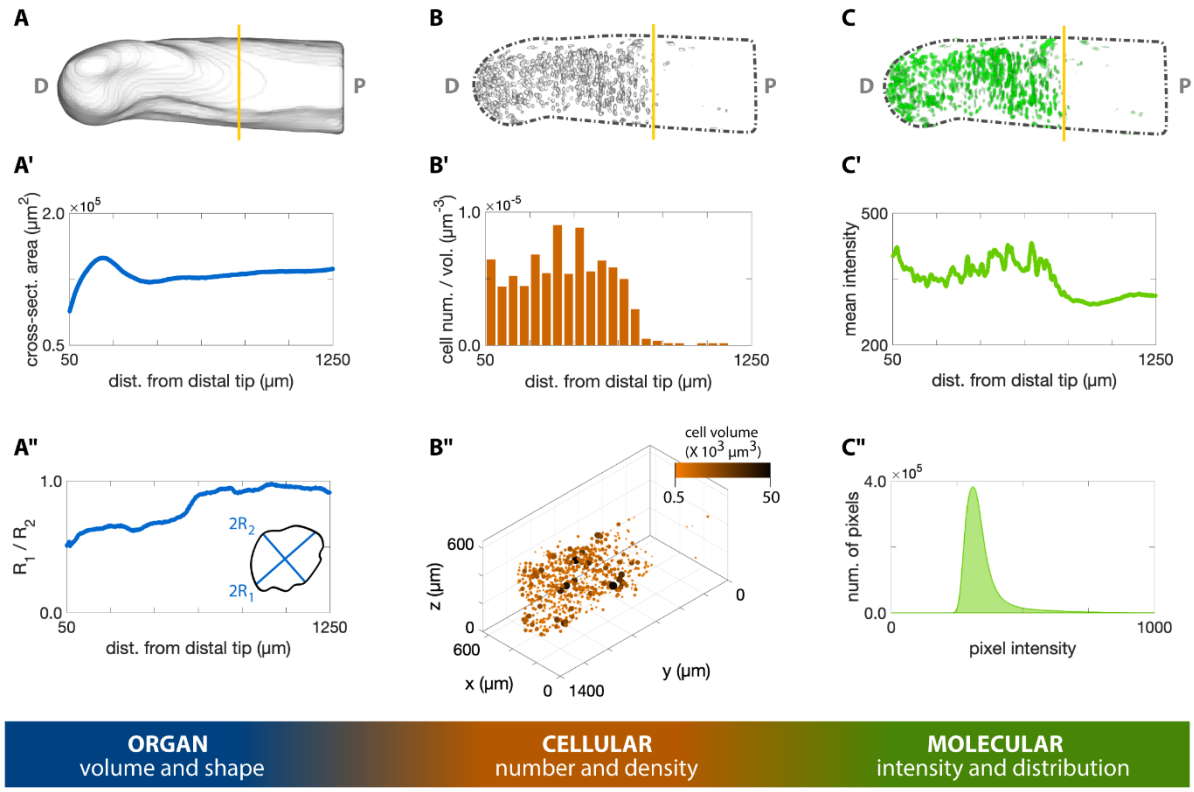

Figure 4. 3D quantification across scales of a regenerating axolotl humerus.

(A) The cross-sections of the humerus in Figure 3D were analyzed with the Fiji plugin BoneJ to quantify humerus shape and volume. (A') The cross-sectional area along the proximodistal (P-D) axis provides a measure of volume distribution along the humerus. (A") The ratio of the maximum chord length from the minor axis ($2R_1$) with respect to the maximum chord length from the major axis ($2R_2$) provides a measure of cross-sectional circularity in the humerus. Values closer to 1.0 in the proximal side indicate a more circular cross-section in this zone. (B) The Fiji plugin Trainable Weka Segmentation 3D and 3D Objects Counter were used in the cellular analysis of proliferating chondrocytes illustrated in Figure 3E. (B') The number of EdU^+ cells within a 50μm slice along the P-D axis was divided by the slice volume to obtain a density-like measure. (B") The center of mass of each cell was plotted in 3D, with point size and color proportional to the segmented cell volume. (C) The molecular intensity and distribution were analyzed based on the resliced pixel intensity maps of the masked green channel in Figure 3F. (C') Mean intensity of each slice perpendicular to the P-D axis. (C") The histogram of the EdU

475 staining in the humerus can provide a measure of DNA synthesis rate. The vertical yellow line in
476 the top row images indicates the plane of amputation.

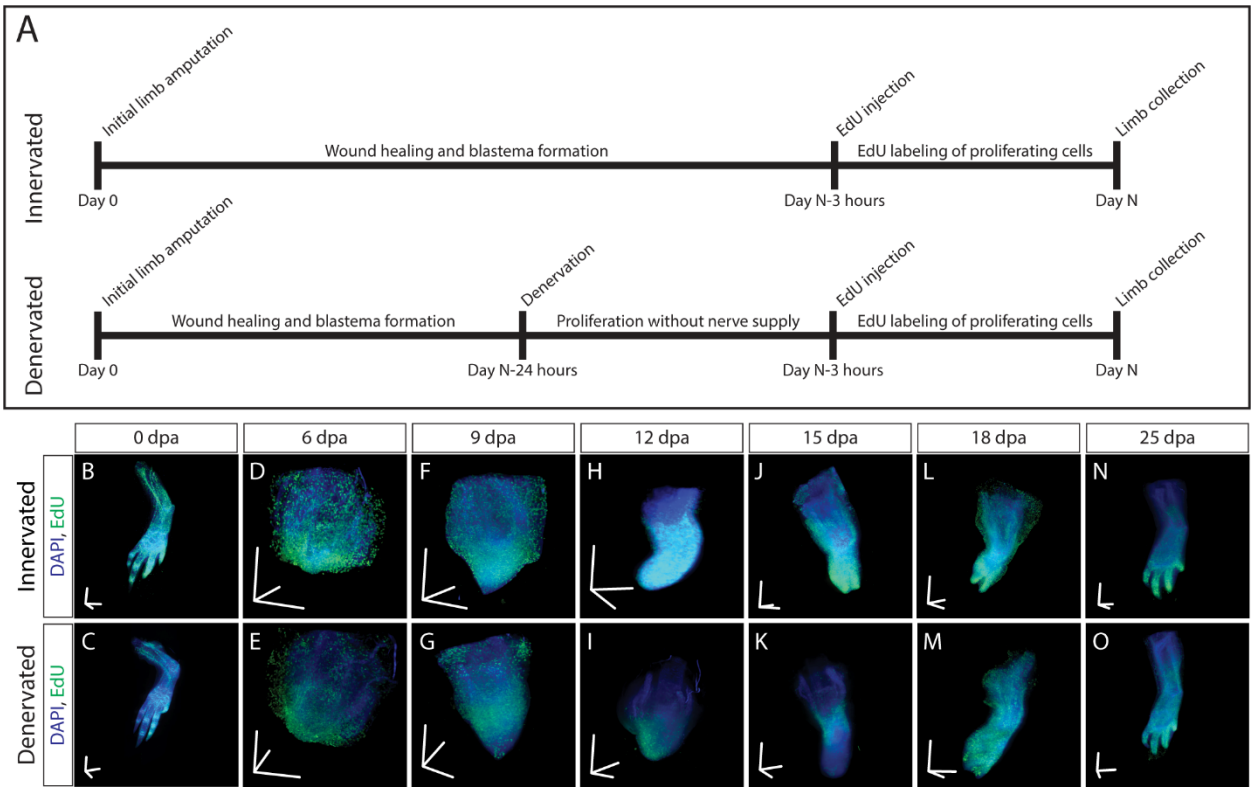

477 **Figure 5. 3D visualization of DNA synthesis in innervated/denervated regenerating limbs.**

478 (A) Schematic of experimental design used to obtain samples from B-O. (B-O) Time course of
479 regeneration in innervated and 24 hour denervated limbs at 0, 6, 9, 12, 15, 18, and 25 dpa. Scale
480 bars for panels B-O=600µm for each axis.

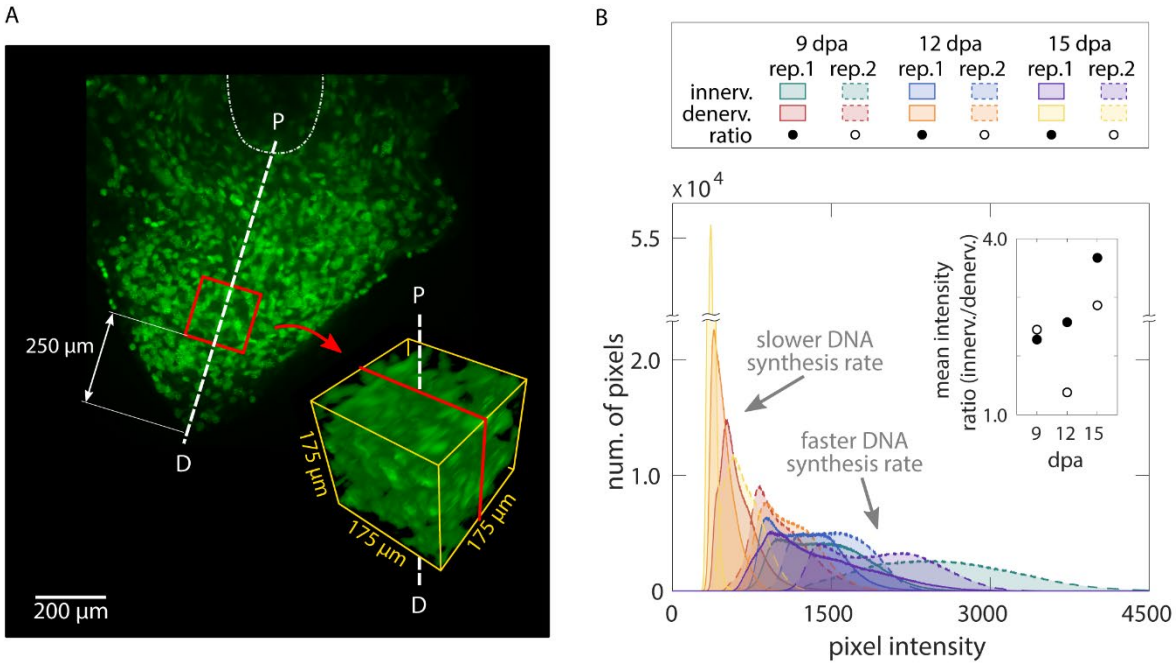

481 **Figure 6. 3D quantification of DNA synthesis in innervated/denervated regenerating limbs.**

482 (A) A cube with sides of 175µm was cropped along the proximodistal axis 250µm from the
483 distal tip of each blastema. (B) The overall histogram of the cubes confirms that innervated
484 blastemas have faster DNA synthesis rates than their denervated counterparts. The difference is
485 quantified by computing the ratio between the mean pixel intensity of the innervated versus
486 denervated blastema cube of a same animal (inset plot).

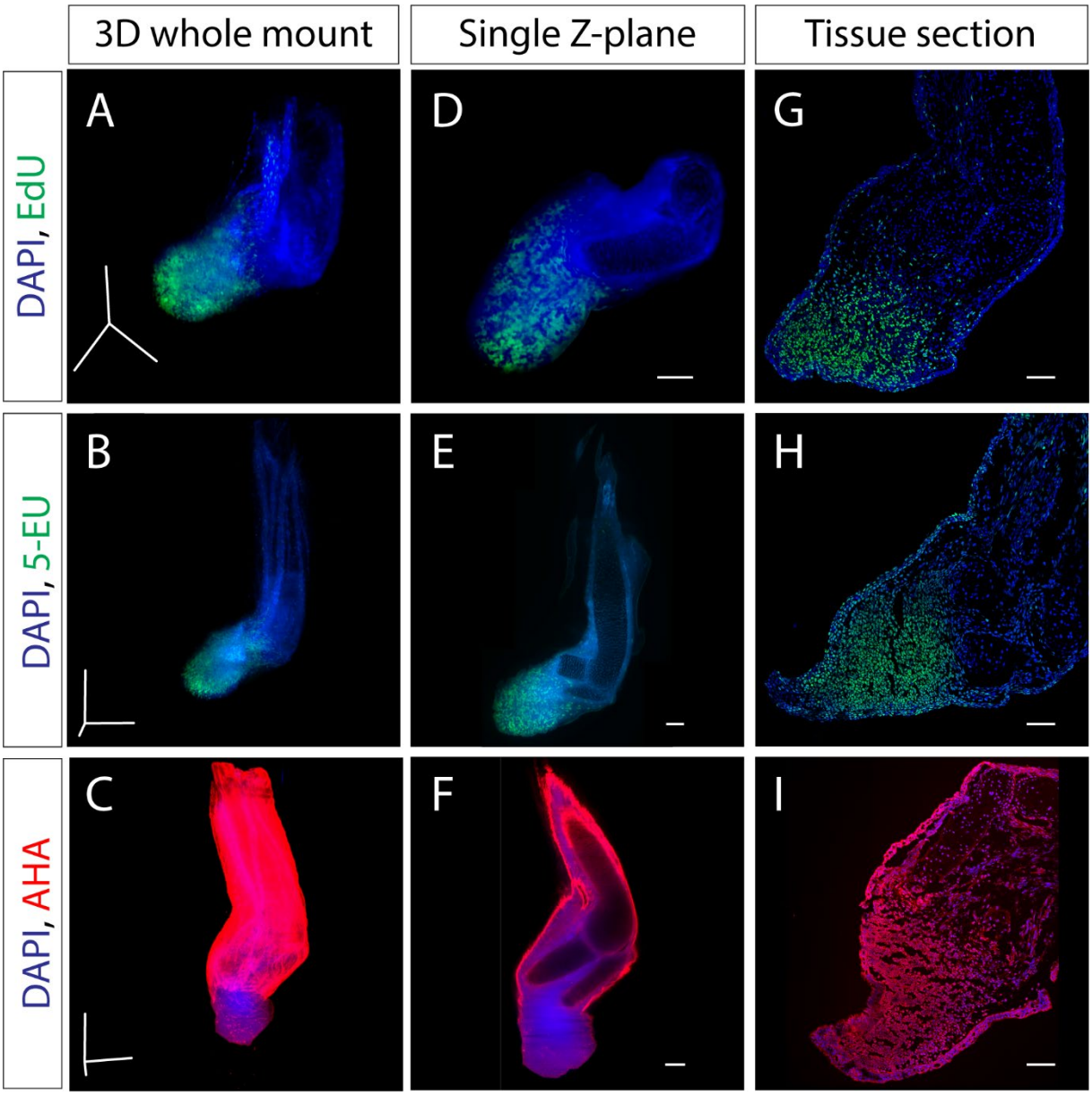

487 **Supplementary figure 1. Single staining of macromolecule synthesis in whole mount.**

488 (A-C) Stitched and fused 3D reconstruction of 13 dpa blastemas stained for one macromolecule
489 obtained by LSFM. (D-F) Single Z-plane from A-C that represents the entirety of the blastema.
490 (G-I) Tissue section from identically treated limbs as A-F. Scale bars for panels A-C= 600µm in
491 each axis. Scale bars for panels D-I= 200µm.

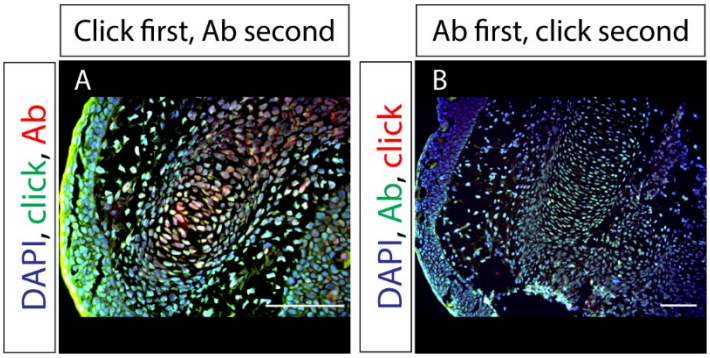

492 **Supplementary figure 2. Specificity of GlcNAz staining.**

493 (A) Tissue section of a regenerating axolotl limb where the click-it cocktail (green) for GlcNAz
494 was applied prior to staining with GlcNAc antibodies (Ab) (red). (B) Tissue section of a
495 regenerating axolotl limb where GlcNAc antibodies (green) were applied prior to treatment with
496 the click-it cocktail (red) for GlcNAz, demonstrating the specificity of the *in vivo* GlcNAz
497 labeling. Scale bars=100µm.

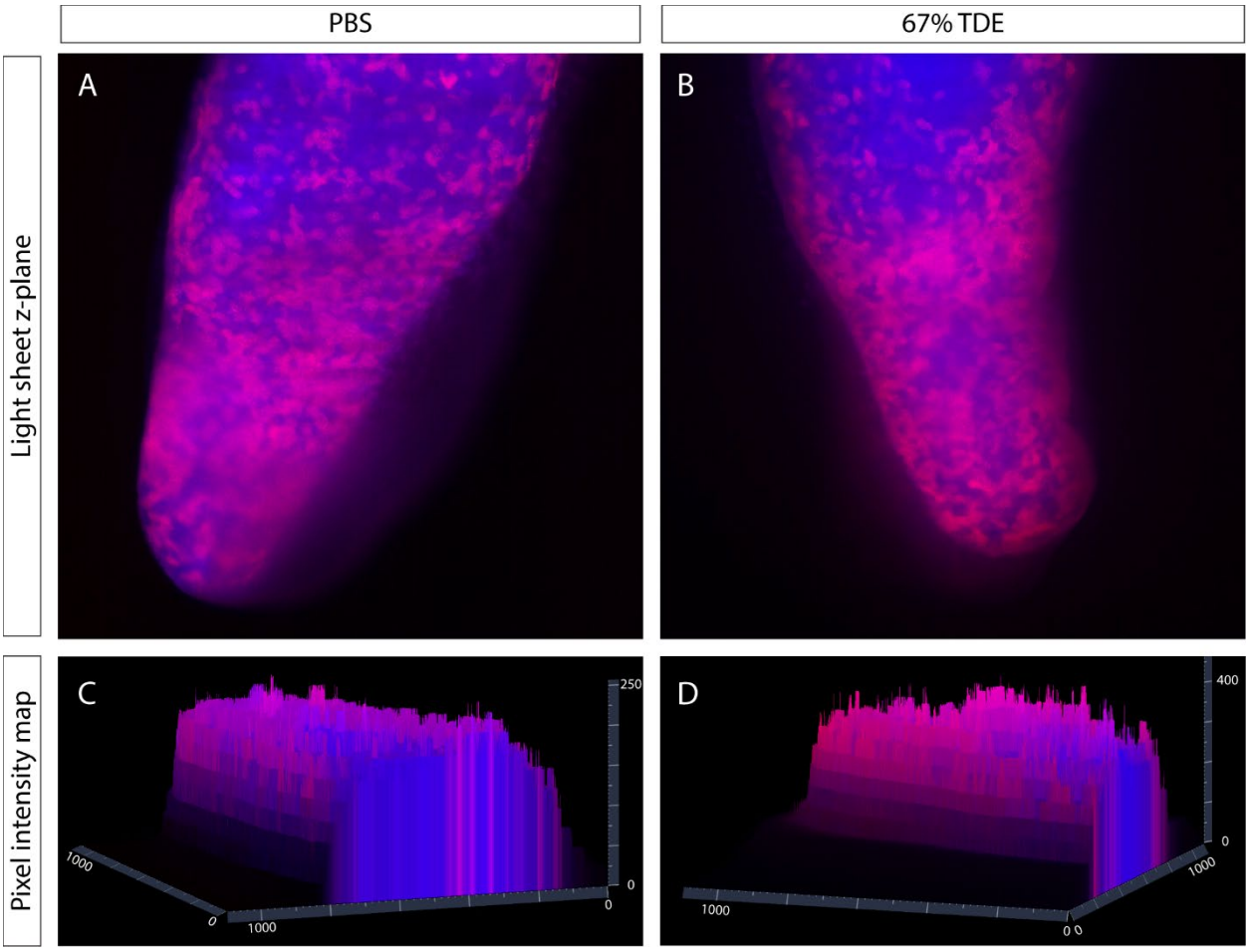

498 **Supplementary figure 3. Comparison of imaging in PBS and 67%TDE**

499 (A-B) Single Z-plane of 13 dpa blastema imaged in PBS (A) or cleared and imaged in 67% TDE
500 (B). Red indicates EdU staining whereas blue represents DAPI staining. (C-D) Pixel intensity
501 map of PBS imaged blastema (C) and 67% TDE imaged blastema (D). Scale bars are in units of
502 microns.

503 **Supplementary video 1**

504 Rotating axolotl hand stained for EdU (green) and GlcNAz (red).

505 **Supplementary video 2**

506 Rotating axolotl limb stained for EdU (green), AHA (red), and DAPI (blue).

507 **Supplementary video 3**

508 Scroll through of Z-stack from supplementary video 2.